ISTITUTO NAZIONALE DI FISICA NUCLEARE

Sezione di Milano

INFN/TC-96/15
2 Ottobre 1996

G. Ambrosio, G. Bellomo:

MAGNETIC FIELD, MULTIPOLE EXPANSION AND PEAK FIELD IN 2D FOR SUPERCONDUCTING ACCELERATOR MAGNETS

PACS: 85.25.Am

SIS–Pubblicazioni
dei Laboratori Nazionali di Frascati

INFN – Istituto Nazionale di Fisica Nucelare
Sezione di Milano – Laboratorio Acceleratori e Superconduttività Applicata

INFN/TC-96/15
2 Ottobre 1996

MAGNETIC FIELD, MULTIPOLE EXPANSION AND PEAK FIELD IN 2D FOR SUPERCONDUCTING ACCELERATOR MAGNETS.

G. Ambrosio and G. Bellomo
Dipartimento di Fisica dell'Universitá di Milano, INFN–Sezione di Milano
Laboratorio LASA, via Fratelli Cervi 201, 20090 Segrate (Milano) – I

ABSTRACT

Superconducting magnets (dipoles,quadrupoles,..) for large accelerators have field properties depending essentially on their straight section part owing to the large length over aperture ratio.

The magnetic field can therefore be computed in 2D with good accuracy using analytical formulas and few simple approximations (uniform current density in the coils, constant iron permeability in a cylindrical yoke).

In this report analytical formulas, based on the complex contour integral technique, are presented for the calculation of the multipole coefficients in the magnet aperture and of the magnetic field inside the coils. The formulas are quite general and specific examples are given for magnets with rectangular or shell coils.

A comparison with advanced codes is done for a test case in order to evaluate the influence of the assumptions on the computed field characteristics of a magnet.

Contents

Symbols

$A(z_0)$	vector potential in z_0,
$V(z_0)$	scalar potential in z_0,
$B(z_0)$	$=B_x + iB_y$ complex magnetic field in z_0,
$B^*(z_0)$	$=B_x - iB_y$ complex conjugate of B,
a_n	skew multipole coefficient of magnetic field,
b_n	normal multipole coefficient of magnetic field,
c_n	$=a_n - ib_n$ complex magnetic field multipole coefficient,
$c_{n,iron}$	multipole coefficient of iron contribution to magnetic field,
$\tilde{a}_n$	normalized skew multipole coefficient,
$\tilde{b}_n$	normalized normal multipole coefficient,
$\tilde{c}_n$	$=\tilde{a}_n - i\tilde{b}_n$,
i	$=\sqrt{-1}$,
I	current,
J	current density,
R	iron yoke inner radius,
R_r	reference radius for multipole coefficients normalization,
z_0	point where magnetic field is calculated,
z	any point in complex plane,
z^*	z complex conjugate,
z_k	coil vertex,
γ	coil contour,
μ_0	vacuum permeability coefficient,
μ_r	iron relative permeability coefficient,
σ	coil cross-section.

Nomenclature for each path and each coil is shown in figures.

1 INTRODUCTION

There are many kinds of superconducting magnets for accelerators (dipoles, quadrupoles, sextupoles, ...) and many different models have been built for each kind. All of them have some fundamental features in common (see fig 1):

- in their centre there is a bore for the beam (the 'aperture')
- the conductors run parallel to the beam over the longest part of the magnet (the 'straight section') and turn in two short end sections (the 'heads')
- there is a non magnetic collar to withstand the Lorentz forces
- there is an iron yoke used to increase the magnetic field inside the aperture and to reduce the fringe field outside the magnet.

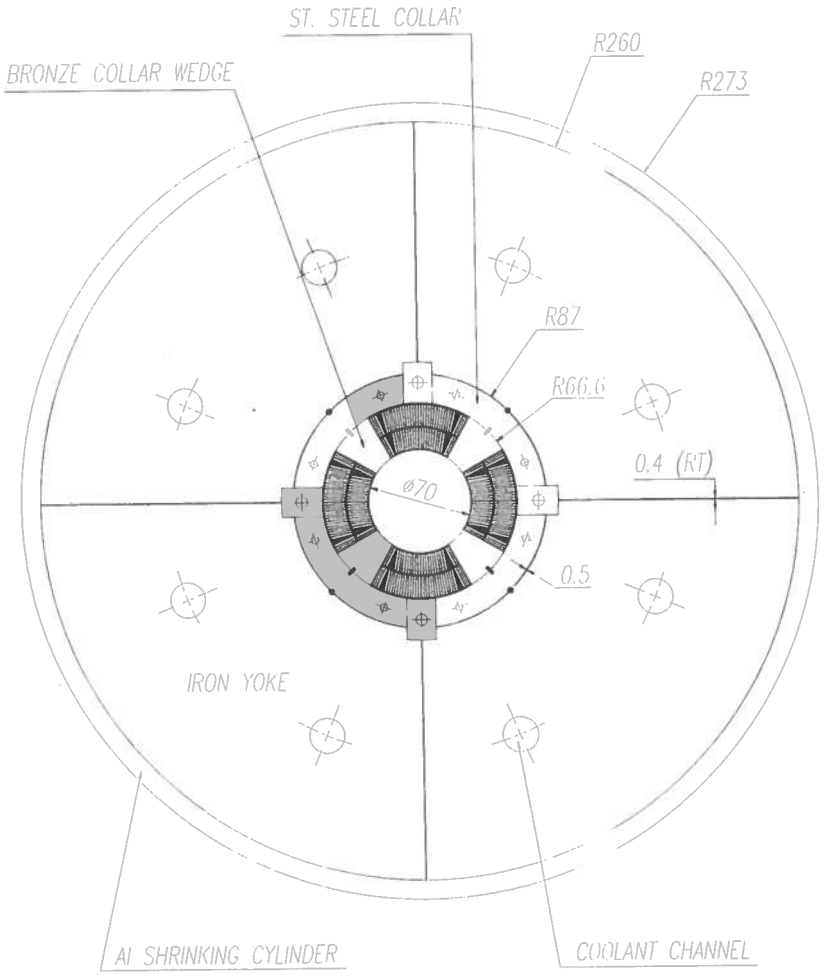

FIG. 1: Cross-section of a quadrupole (from ref 1).

The magnetic field properties are essentially given by the straight section part of the magnet, owing to the large length/aperture ratio (typical values: aperture 50-100 mm, length 1-10 m), and are dominated by the coils contribution (up to 90% of the total field).

The magnetic field can therefore be computed with good accuracy in 2D. Analytical formulas, particularly useful in the initial design stage, can be developed with few simple approximations:

- uniform current density in the coils
- constant iron permeability in a cylindrical yoke

These analytical formulas have been developed and applied to the study of a superconducting Nb_3Sn quadrupole [1] for the *low* β insertions of LHC at CERN.

In this report the technique of contour integrals in complex field is developed to compute magnetic field outside and inside coils and multipole coefficients in the magnet aperture. This technique has been used by many authors,for instance Beth[2] , Halbach[3] and Brechna[4] . Here we follow closely the approach of Halbach.

The basic notation for the complex field and the multipole field expansion in the aperture are given in sect. 2 and sect. 3 respectively while in sect. 4 it is shown how to evaluate (with the method of the image current) the contribution of a cylindrical iron yoke with constant permeability.

The symmetries of a magnet (midplane and rotational) are considered in sect. 5 to reduce the calculation effort and to obtain a magnet with minimal high order multipole coefficients. Explicit evaluation of multipole coefficients are presented in sect. 6 for coils with rectangular or circular shape including the iron contribution.

The complex line integral technique is introduced in sect. 7 in order to evaluate the field and the multipole coefficients for the most general coil shape (boundary delimited by straight lines and/or circular arcs). The calculation of the magnetic field inside the coils is presented in sect. 8 and it is also shown that the peak value (modulus) of the field is reached on the coil boundary. Evaluation of some fundamental line integrals for these kind of paths and applications to various coil shape are presented in sect. 9.

Finally a test case, and a comparison with other more advanced codes, is presented in sect. 10 to show the effect of the approximations (uniform current density in the coils and constant iron permeability) on the main parameter of a magnet i.e. the multipole coefficients in the aperture and the peak field value on the coils.

2 COMPLEX MAGNETIC FIELD

The magnetic field modulus in a point z_0 (belonging to the X-Y plane; see fig. 2) generated by an infinite line current I flowing in the Z-axis direction, crossing in z the X-Y plane, is

$$\mid B(z_0) \mid = \frac{\mu_0 I}{2\pi d} \tag{1}$$

where d is the distance between z_0 and z. Since $B_z = 0$ the field may be expressed by the complex number $B = B_x + iB_y$ as a function of the source point $z = x + iy$ and of the field point $z_0 = x_0 + iy_0$. Vector $\vec{B}$ is perpendicular to the segment $z\bar{z}_0$ and the complex field B can be obtained multiplying the modulus by $i(z_0 - z)/ \mid z_0 - z \mid$, which is the versor perpendicular to $z\bar{z}_0$.

$$B = B_x + iB_y = \frac{\mu_0 I}{2\pi \mid z_0 - z \mid} \frac{i(z_0 - z)}{\mid z_0 - z \mid} = \frac{\mu_0 I}{2\pi} \frac{i}{z_0^* - z^*} \tag{2}$$

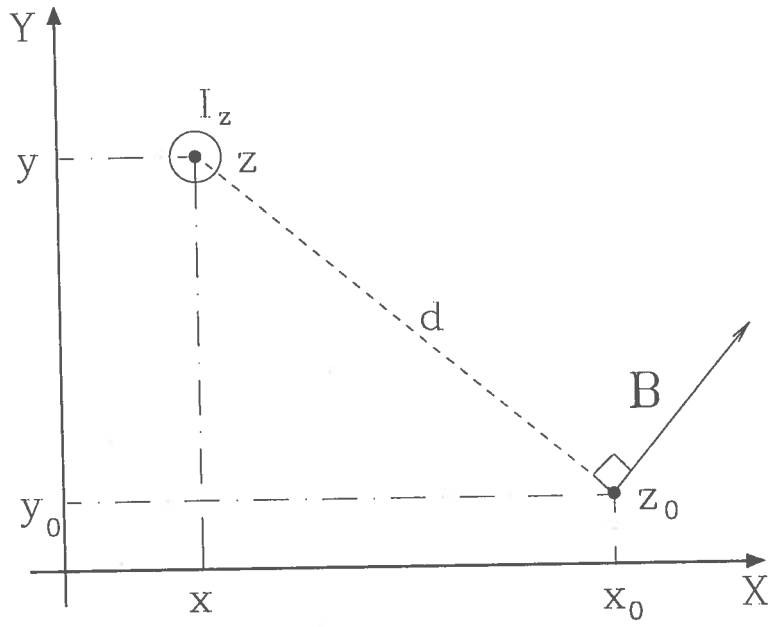

FIG. 2: Field of an infinite line current.

In the last identity z_0^* and z^* are the complex conjugates of z_0 and z.

Since $(i/(a+ib))^* = i/-(a+ib)^*$ the complex conjugates of the field is

$$B^* = B_x - iB_y = \frac{\mu_0 I}{2\pi}\frac{i}{z-z_0} \tag{3}$$

In a more general case the field generated by a current distribution of arbitrary cross section (σ) and uniform density (J) is obtained by integration:

$$B^*(z_0) = i\frac{\mu_0 J}{2\pi}\int_\sigma \frac{1}{z-z_0}\,da \tag{4}$$

The introduction and use of B^* instead of B is due to the fact that $B^*(z_0)$ is an analytic function where J=0, while $B(z_0)$ is never analytic. Analytic functions are quite useful in this kind of calculations since :

- they can be expanded in power series
- for a given region the maximum value of the modulus is on the boundary

The first property of B^* is used for multipole expansion of the field, the second to search for the maximum field point inside the coils. (B^* isn't analytic inside coils, but an equivalent analytic function can be defined; see section 8)

To prove that B^* is analytic is sufficient to show that it satisfies the Cauchy-Riemann's equations, i.e. for the complex function $f(z) = u(x,y) + iv(x,y)$

$$\begin{aligned}\frac{\partial u}{\partial x} &= \frac{\partial v}{\partial y}\\ \frac{\partial u}{\partial y} &= -\frac{\partial v}{\partial x}.\end{aligned} \tag{5}$$

In the case of B^* the first corresponds to $div\,\vec{B} = 0$ while the second holds when $(rot\,\vec{B})_z = 0$ that is where $J_z = 0$.

Another method to prove that B^* is analytic is to use the complex potential $P = A + iV$ (where $A = A_z$ is the vector potential and V is the scalar potential) showing that it satisfy the Cauchy-Riemann equations in the regions where both A and V are defined (i.e. where $J_z = 0$). Therefore also its derivative is an analytic function in the region where P is analytic:

$$\frac{\partial P}{\partial z} = \frac{\partial A}{\partial x} + i\frac{\partial V}{\partial x} = \frac{\partial V}{\partial y} - i\frac{\partial A}{\partial y} = -iB^* \tag{6}$$

3 MULTIPOLE EXPANSION OF THE FIELD

The complex field B* is analytic where J=0 and can be therefore expanded in power series of z. The largest circle centered on the origin (beam axis) not including currents is normally defined as the 'aperture' of the magnet. For each point z_0 of the aperture and all source points (z) of the coils (σ) it is $\mid z_0/z \mid < 1$ and therefore:

$$\frac{1}{z - z_0} = \frac{1}{z}\sum_{n=0}^{\infty}\left(\frac{z_0}{z}\right)^n = \sum_{n=1}^{\infty}\frac{z_0^{n-1}}{z^n} \tag{7}$$

The field (4) in the aperture is given as:

$$B^*(z_0) = \sum_{n=1}^{\infty} c_n z_0^{n-1} \tag{8}$$

$$c_n = \frac{i\mu_0 J}{2\pi}\int_\sigma \frac{1}{z^n}\,da \tag{9}$$

The c_n are the multipole coefficients (not normalized); c_1 is called the dipole coefficient, c_2 and c_3 the quadrupole and the sextupole, etc. These definitions show that in a 2N-pole magnet the main multipole coefficient (the only one in ideal case) is c_N. The real and imaginary part of these coefficients are usually defined as:

$$c_n = a_n - ib_n \tag{10}$$

The b_ns generate vertical fields (B_y) on the midplane $(y = 0)$ and are called "right components", while the a_ns generate horizontal fields on the same plane and are called "skew components".

The multipole coefficients, as defined in equ. 9, are dimensional and are not very useful to express the field quality of a magnet nor to compare similar magnets. For these reasons normalized dimensionless multipole coefficients $\tilde{a}_n$ and $\tilde{b}_n$ are introduced rewriting the field expansion as

$$iB^* = B_y + iB_x = B_0\sum_{n=1}^{\infty}(\tilde{b}_n + i\tilde{a}_n)\left(\frac{z_0}{R_r}\right)^{n-1} \tag{11}$$

where (R_r) is a reference radius, generally chosen as 2/3 of the aperture, and B_0 is the main right multipole field, i.e. $B_0 = b_1$ for a dipole, $B_0 = b_2 R_r$ for a quadrupole, etc. To obtain $\tilde{b}_n$ and $\tilde{a}_n$ from c_n we can see that:

$$iB^*(z_0) = \sum_{n=1}^{\infty} ic_n z_0^{n-1} = B_0\sum_{n=1}^{\infty}\left(ic_n\frac{R_r^{n-1}}{B_0}\right)\left(\frac{z_0}{R_r}\right)^{n-1} \tag{12}$$

and so:

$$\begin{aligned} \tilde{b}_n &= b_n \frac{R_r^{n-1}}{B_0} \quad (right) \\ \tilde{a}_n &= a_n \frac{R_r^{n-1}}{B_0} \quad (skew) \end{aligned} \tag{13}$$

Superconducting magnets for accelerators normally require multipole components of the order of 10^{-4} of the main ideal field.

It is necessary to note that no standard notation is internationally recognized: for example in USA the multipole notation is different (b_0 is the dipole, b_1 is the quad, etc) while at CERN the reference radius is assumed 1 cm independent of the aperture.

3.1 Multipole expansion in cylindrical coordinates

The multipole coefficients of a magnet are measured with a rotating coil which integrates the B_r component of the field. It is therefore useful a multipole expansion of the field components B_r,B_θ in cylindrical coordinates, which can be easily obtained through a rotation of the field components B_x,B_y. Using the complex notation

$$B_{rot} = B_r + iB_\theta = Be^{-i\theta} = \sum_{n=1}^{\infty}(a_n + ib_n)r^{n-1}e^{-in\theta}. \tag{14}$$

The explicit formulas for the field components are:

$$\begin{aligned} B_r(r,\theta) &= \sum_{n=1}^{\infty} r^{n-1}[a_n cos(n\theta) + b_n sin(n\theta)] \\ B_\theta(r,\theta) &= \sum_{n=1}^{\infty} r^{n-1}[-a_n sin(n\theta) + b_n cos(n\theta)] \end{aligned} \tag{15}$$

These formulas can also be obtained[5] alternatively by expansion, in cylindrical coordinates, of the vector potential A.

The pattern of the magnetic field (B_n) generated by each multipole component can be easily recognized: each component a_n or b_n generates magnetic field components growing as r^{n-1} and oscillating azimuthally as $n\theta$.

3.2 Multipole expansion of the potentials

We have already seen that in a 2D problem it's possible to define a complex potential $P = A + iV$ that is an analytic function: $B^* = i\partial P/\partial z$. It can be expanded in power series:

$$P(z_0) = \sum_{n=1}^{\infty}(d_n + ie_n)z_0^n \tag{16}$$

and this property can be used to obtain the multipole expansions of A and V. Writing $z_0 = r\ exp(i\theta)$ they are:

$$A_z(z_0) = ReP(z_0) = \sum_{n=1}^{\infty} r^n[d_n cos(n\theta) - e_n sin(n\theta)] \tag{17}$$

$$V(z_0) = ImP(z_0) = \sum_{n=1}^{\infty} r^n[e_n cos(n\theta) + d_n sin(n\theta)] \tag{18}$$

To obtain the relations between the multipole coefficients of the potentials (d_n, e_n) and those of the field (b_n, a_n), it can be noted that

$$iB^*(z_0) = -\frac{\partial P}{\partial z} = -\sum_{n=1}^{\infty}(d_n + ie_n)nz_0^{n-1} \tag{19}$$

and making a comparison with equ. 8 we find

$$\begin{aligned} b_n &= -n\, d_n \quad (right) \\ a_n &= -n\, e_n \quad (skew) \end{aligned} \tag{20}$$

These formulas are normally used in the numerical codes for magnetostatic problem. They solve the problem for the vector potential A_z, and the multipole coefficients of the field B are computed through the multipole expansion of the potential A_z.

The code POISSON[9] uses a normalized expansion of the vector potential:

$$A_z(z_0) = Re\left\{\sum_{n=1}^{\infty}(\tilde{d}_n + i\tilde{e}_n)\left(\frac{z_0}{R_r}\right)^n\right\} \tag{21}$$

and the normalized multipole coefficients of the field $\tilde{b}_n, \tilde{a}_n$ are:

$$\begin{aligned} \tilde{b}_n &= -\tilde{d}_n \frac{n}{B_0 R_r} \\ \tilde{a}_n &= -\tilde{e}_n \frac{n}{B_0 R_r}. \end{aligned} \tag{22}$$

4 CIRCULAR IRON SCREEN

The contribution to the field of a cylindrical iron yoke can be analyzed with the method of the image current. Assuming a constant iron permeability ($\mu = \mu_r\, \mu_0$) and a hollow iron screen of radius R_{iron} (i.e. ignoring the finite radial extension of the yoke) a line current I at position $z = re^{i\phi}$ is imaged (see fig. 3) in the line current $I' = \frac{\mu_r - 1}{\mu_r + 1} I$ at position $z' = r'e^{i\phi'}$ with $\phi' = \phi$ and $r' = R_{iron}^2/r$.

In the case of a coil the current density (J') of the image coil σ' depends on the distance of the point from the center of the aperture (r'):

$$J'(r') = \frac{\mu_r - 1}{\mu_r + 1}\left(\frac{R_{iron}}{r'}\right)^4 J(r) \tag{23}$$

The field contribution (for $r < R_{iron}$) is given by

$$B^*_{iron}(z_0) = i\frac{\mu_0}{2\pi}\int_{\sigma'}\frac{J'(r')}{z' - z_0}\, da' \tag{24}$$

Using the relations between r, J and r', J', and the fact that $da' = (R_{iron}/r)^4\, da$ the integral over σ' can be transformed in an integral over σ :

$$B^*_{iron}(z_0) = i\left(\frac{\mu_r - 1}{\mu_r + 1}\right)\frac{\mu_0 J}{2\pi}\int_{\sigma}\frac{z^*}{R^2 - z^* z_0}\, da \tag{25}$$

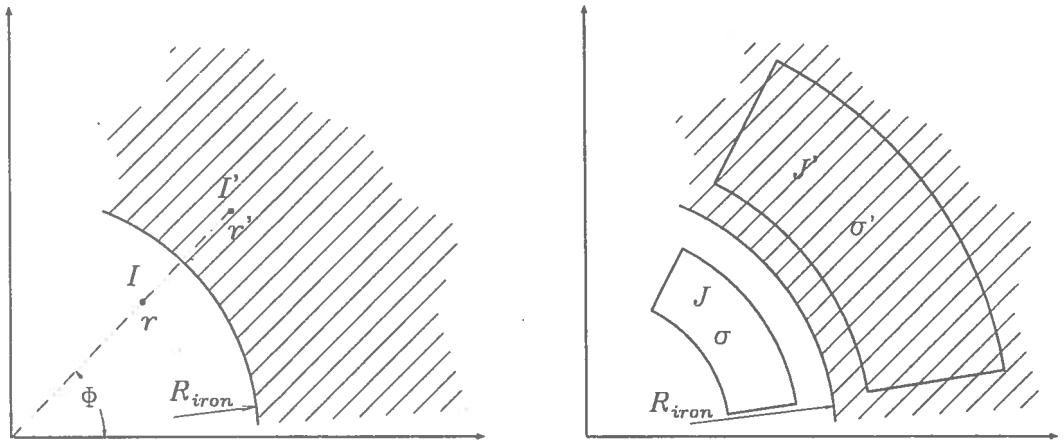

FIG. 3: Image of a line current and of a circular shell.

The iron contribution to the multipole coefficients can be calculated making a Taylor expansion of B^*_{iron}. Since

$$\frac{z^*}{R^2 - z^* z_0} = \frac{z^*}{R^2} \sum_{n=0}^{\infty} \left(\frac{z_0 z^*}{R^2} \right)^n = \sum_{n=1}^{\infty} \frac{(z^*)^n}{R^{2n}} z_0^{n-1} \tag{26}$$

then

$$c_{n,iron} = i \left(\frac{\mu_r - 1}{\mu_r + 1} \right) \frac{\mu_0 J}{2\pi} \int_\sigma \frac{(z^*)^n}{R^{2n}} \, da \tag{27}$$

It's worth noting that a circular iron yoke with constant permeability does not introduce new multipole coefficients in the case of a circular shell coil since the image coil is still a circular shell with the same azimuthal extension (see section 6.2).

At low magnet excitation one can assume $\mu = \infty$ and $\frac{\mu_r - 1}{\mu_r + 1} = 1$. At full excitation the iron is partially saturated: assuming $\mu_r = 5$ as a typical value follows $\frac{\mu_r - 1}{\mu_r + 1} = \frac{2}{3}$, i.e. the saturation of the iron reduces its efficiency to 2/3 respect to the ideal case.

5 SYMMETRY

Superconducting magnets for large accelerators are generally built with a high degree of symmetry.

A 2N-pole magnet has two types of symmetry :

- midplane symmetry ($B_x = 0$ on the plane $Y = 0$)
- azimuthal symmetry (i.e. the coil structure in invariant under rotation by π/N)

The midplane symmetry gives multipole coefficients which are imaginary since on the midplane there is only the field component B_y (i.e. there are only right components).

The azimuthal symmetry allows to calculate the total contribution of the coils using only the basic structure (i.e. the coil, or coils, between two poles; for instance between

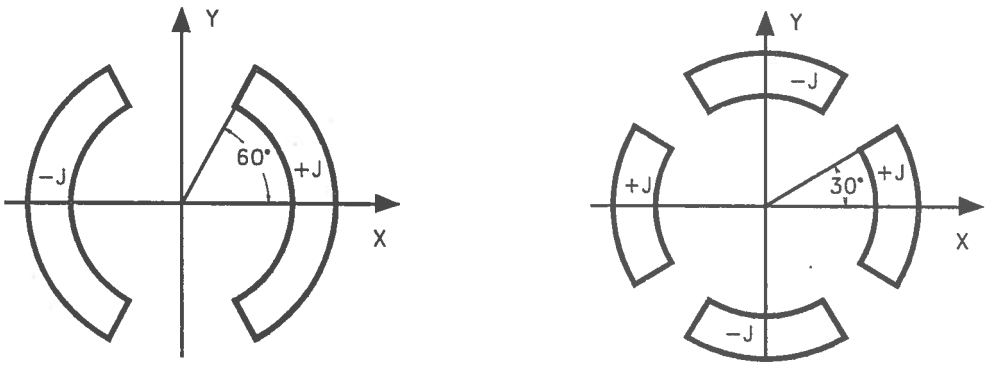

FIG. 4: Dipole and quadrupole with high order compensation, $b_3 = 0$ for the dipole, $b_6 = 0$ for the quadrupole.

$-\pi/2$ and $\pi/2$ in a dipole, and between $-\pi/4$ and $\pi/4$ in a quadrupole). In fact a rotation by an angle α of this coil gives :

$$c_n(\alpha) = c_n(0)e^{-in\alpha} \tag{28}$$

(where $c_n(0)$ is the multipole coefficient due to the coil in the original position) and therefore the multipole coefficient due to the whole magnet (i.e. all coils with alternated sign of the current density) is:

$$c_{n,total} = c_n(0)\sum_{j=1}^{2N}(-1)^j e^{-inj\frac{\pi}{N}} \tag{29}$$

It follows then

$$c_{n,tot} = \begin{cases} 2Nc_n(0) & \text{if } n = (2k+1)N \quad k = 0,1,2,... \\ 0 & \text{otherwise} \end{cases} \tag{30}$$

For example in a dipole built with the aforementioned azimuthal symmetry the only non vanishing coefficients are $c_1, c_3, c_5, c_7, ...$ while for a quadrupole the allowed coefficients are $c_2, c_6, c_{10}, c_{14}, ...$

If in addition the magnet has midplane symmetry all the allowed coefficients are imaginary (i.e. there are only right coefficients) and the basic structure can be reduced. In fact in this case it's possible to study only half a coil (for instance the part between 0 and $\pi/2$ in a dipole or between 0 and $\pi/4$ in a quadrupole) because the multipole coefficients of the whole magnet are given by:

$$b_{n,tot} = \begin{cases} 4Nb_n(0) & \text{if } n = (2k+1)N \quad k = 0,1,2,... \\ 0 & \text{otherwise} \end{cases} \tag{31}$$

where $b_n(0)$ are the right components of the half coil.

Selection of particular coil shape, or combinations of various coils, can be used to cancel the high order coefficients. In the case of circular shell coils, it can be easily shown that in a 2N-pole magnet the first high order coefficient (b_3 for dipoles, b_6 for quadrupoles,...) can be canceled choosing for the coil an azimuthal extension of $2\pi/3N$. These structures are shown in fig. 4 for the case of dipoles and quadrupoles.

For rectangular coils the only practical way to eliminate the first high order harmonic is to place a wedge on the midplane.

More elaborate schemes are found in the literature for the compensation of high order harmonics:

- multiple coils in the same layer
- use of multiple layers with an higher current density in the external layer ('grading')
- insertion of wedges in the layers (equivalent to have multiple coils and multiple layers.)

Examples of high order multipole compensation for a quadrupole with rectangular or shell coils are presented in fig. 5 (from ref 1).

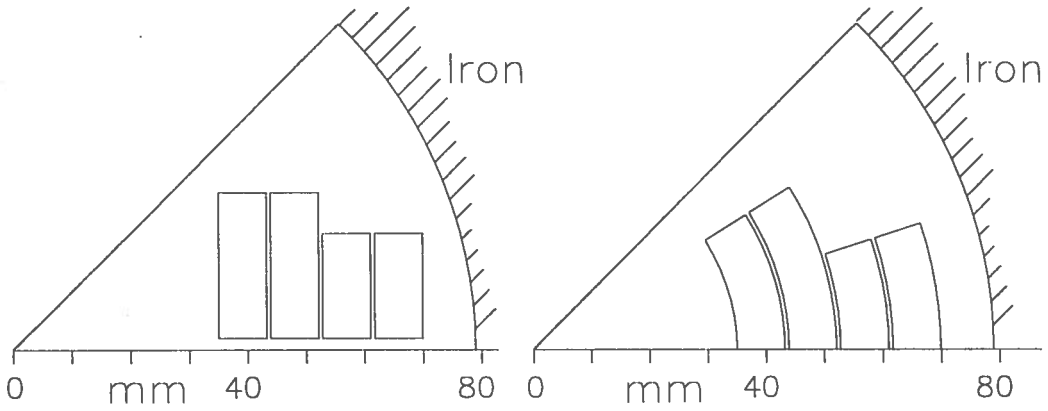

FIG. 5: High order multipole compensation for a quadrupole with rectangular or shell coils.

6 EXAMPLES

6.1 Rectangular coils with midplane symmetry

The multipole coefficients of a rectangular coil with midplane symmetry can be easily calculated using equ 9. Because of the symmetry no skew multipoles are expected. All symbols in the following formulas are shown in fig. 6.

$$\begin{aligned} c_1 &= \frac{i\mu_0 J}{2\pi}\int_{x_1}^{x_2}\int_{-h}^{h}\frac{1}{x+iy}\,dy\,dx = \frac{\mu_0 J}{2\pi}\left[(x+ih)\,ln(x+ih)-(x-ih)\,ln(x-ih)\right]_{x_1}^{x_2} \\ &= \frac{\mu_0 J}{2\pi}\left[x_2 ln\left(\frac{x_2+ih}{x_2-ih}\right)-x_1 ln\left(\frac{x_1+ih}{x_1-ih}\right)+ih\,ln\left(\frac{(x_2+ih)(x_2-ih)}{(x_1+ih)(x_1-ih)}\right)\right] \\ &= \frac{i\mu_0 J}{\pi}\left[x_2\alpha_2 - x_1\alpha_1 + h\,ln\left(\frac{r_2}{r_1}\right)\right] \end{aligned} \tag{32}$$

$$\begin{aligned} c_2 &= \frac{i\mu_0 J}{2\pi}\int_{x_1}^{x_2}\int_{-h}^{h}\frac{1}{(x+iy)^2}\,dy\,dx = \frac{-\mu_0 J}{2\pi}\left[ln\left(\frac{x+ih}{x-ih}\right)\right]_{x_1}^{x_2} \\ &= \frac{i\mu_0 J}{\pi}(\alpha_1-\alpha_2) \end{aligned} \tag{33}$$

$$
\begin{aligned}
c_{n>2} &= \frac{\mu_0 J}{2\pi(n-2)(n-1)}\left[\frac{1}{(x+ih)^{n-2}} - \frac{1}{(x-ih)^{n-2}}\right]_{x_1}^{x_2} \\
&= \frac{\mu_0 J}{2\pi(n-2)(n-1)}\left(\frac{e^{-i(n-2)\alpha_2} - e^{i(n-2)\alpha_2}}{r_2^{n-2}} - \frac{e^{-i(n-2)\alpha_1} - e^{i(n-2)\alpha_1}}{r_1^{n-2}}\right) \\
&= \frac{i\mu_0 J}{\pi(n-2)(n-1)}\left(\frac{sin[(n-2)\alpha_1]}{r_1^{n-2}} - \frac{sin[(n-2)\alpha_2]}{r_2^{n-2}}\right) \qquad (34)
\end{aligned}
$$

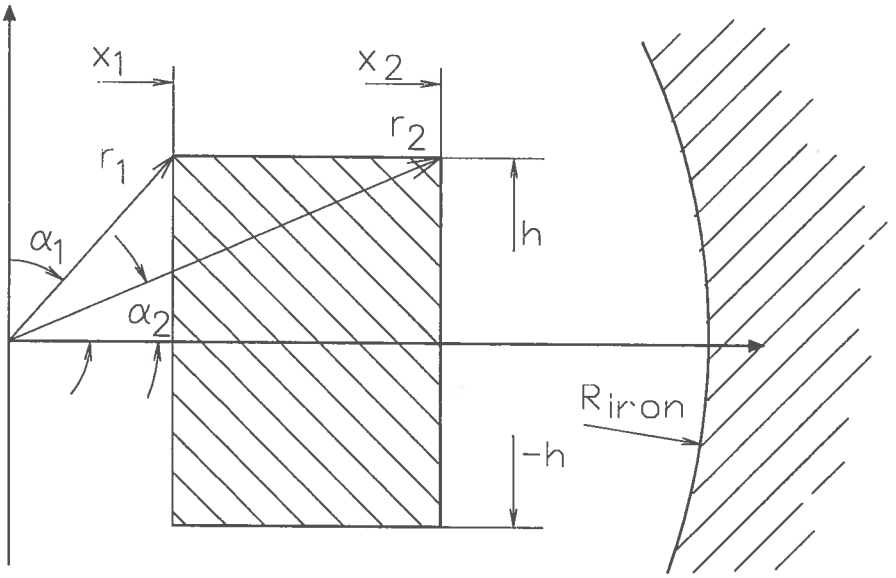

FIG. 6: Rectangular coil with midplane symmetry.

The iron contribution to each multipole coefficients is (using formula 27):

$$
c_{n,iron} = i\left(\frac{\mu_r - 1}{\mu_r + 1}\right)\frac{\mu_0 J}{\pi}\left(\frac{r_2^{n+2} sin[(n+2)\alpha_2] - r_1^{n+2} sin[(n+2)\alpha_1]}{(n+2)(n+1)R^{2n}}\right) \qquad (35)
$$

6.2 Circular shell coils with midplane symmetry

Here we report the multipole coefficients of a circular shell coil symmetric respect to the midplane[6] . See fig. 7 for an example and nomenclature. Like in the previous case all coefficients have no real part because of coil symmetry.

$$
c_{n>2} = \frac{i\mu_0 J}{2\pi}\int_{r_1}^{r_2}\int_{-\alpha}^{\alpha}\rho^{-n}e^{-in\theta}\rho\; d\rho\, d\theta = \frac{i\mu_0 J}{\pi n(2-n)}\left(r_2^{2-n} - r_1^{2-n}\right)sin(n\alpha) \qquad (36)
$$

$$
c_2 = \frac{i\mu_0 J}{2\pi} ln\left(\frac{r_2}{r_1}\right) sin(2\alpha) \qquad (37)
$$

$$
c_1 = \frac{i\mu_0 J}{\pi}(r_2 - r_1)sin(\alpha). \qquad (38)
$$

The iron contribution to the multipole coefficients is:

$$
c_{n,iron} = i\left(\frac{\mu_r - 1}{\mu_r + 1}\right)\frac{\mu_0 J}{\pi R_{iron}^{2n}}\left(\frac{r_2^{n+2} - r_1^{n+2}}{n(n+2)}\right)sin(n\alpha) \qquad (39)
$$

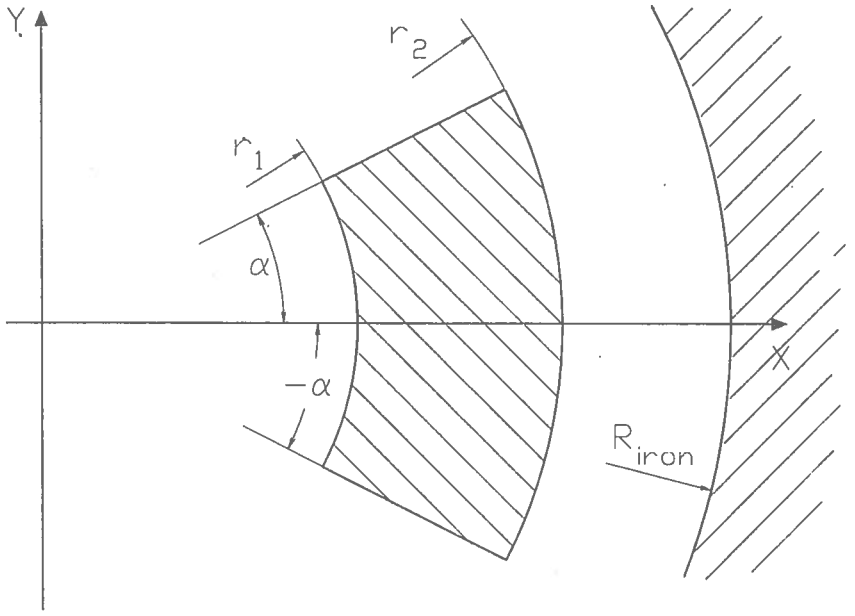

FIG. 7: Circular shell coil with midplane symmetry.

We note that the cylindrical yoke does not introduce new multipole coefficients since its multipoles show the same $sin(n\alpha)$ dependence as those of the coil.

7 FROM SURFACE INTEGRALS TO CONTOUR INTEGRALS

All integrals used above to calculate magnetic field and multipole coefficients are surface integrals. These integrals become cumbersome and difficult to solve when studying generic shape coils.

It is possible to transform them in contour integrals using a particular form of the Stokes theorem, known also as Green theorem in complex field[3, 7] :

$$\int_\sigma \frac{\partial F}{\partial z^*}\, da = \frac{1}{2i}\oint_\gamma F\, dz \tag{40}$$

$$\int_\sigma \frac{\partial F}{\partial z}\, da = -\frac{1}{2i}\oint_\gamma F\, dz^* \tag{41}$$

In these formulas F and its first derivatives should be single-valued and with no singularities in the integration area (σ); γ is the contour of σ and must be covered in anticlockwise direction.

The multipole coefficients can be obtained applying equ. 40 and 41 to equations 9 and 27. Here are the two equivalent expressions:

$$c_n = \frac{\mu_0 J}{4\pi}\oint_\gamma \frac{z^*}{z^n}\, dz \quad (n \geq 1) \tag{42}$$

$$c_n = \frac{\mu_0 J}{4\pi}\frac{1}{n-1}\oint_\gamma z^{1-n}\, dz^* \quad (n > 1) \tag{43}$$

The iron contribution to each multipole is:

$$c_{n,iron} = \left(\frac{\mu_r - 1}{\mu_r + 1}\right) \frac{\mu_0 J}{4\pi} \frac{1}{(n+1)R^{2n}} \oint_\gamma (z^*)^{n+1}\, dz \tag{44}$$

The magnetic field generated by any coil with uniform current density can be calculated, outside the coil, applying equ. 40 to equ. 4. Since $\frac{\partial}{\partial z^*}\left(\frac{z^*-z_0^*}{z-z_0}\right) = \frac{1}{z-z_0}$ assuming $F = \frac{z^*-z_0^*}{z-z_0}$ it is:

$$B^*(z_0) = \frac{\mu_0 J}{4\pi} \oint_\gamma \frac{z^* - z_0^*}{z - z_0}\, dz \tag{45}$$

It is not possible to calculate the field inside the coil, since F has a singularity into the integration area.

The integral in equ. 45 can be broken in two pieces and the second piece is equal to zero, for the Cauchy Theorem[7] , since z_0 is outside the coil. The field outside the coil can then be cast in the form:

$$B^*(z_0) = \frac{\mu_0 J}{4\pi} \oint_\gamma \frac{z^*}{z - z_0}\, dz \tag{46}$$

It is however useful to retain the equ. 45 since this form is valid both outside and inside coils as will be shown in section 8.

The field contribution of a circular yoke with constant iron permeability is obtained in the same way, applying equ. 41 to equ. 25 and assuming $F = \frac{zz^*}{R^2 - z_0 z^*}$:

$$B^*_{iron}(z_0) = -\left(\frac{\mu_r - 1}{\mu_r + 1}\right) \frac{\mu_0 J}{4\pi} \oint_\gamma \frac{zz^*}{R^2 - z_0 z^*}\, dz^* \tag{47}$$

8 MAGNETIC FIELD INSIDE COILS

A map of the magnetic field inside the coils is needed to calculate the Lorentz forces. For the design of superconducting magnets it is also fundamental to locate the peak field (in modulus) which set an upper limit on the current (the critical current).

When calculating the field in a point (z_0) belonging to a coil, and generated by the coil itself, it's not possible to use the Green's theorem (see section 7) to transform the surface integral into a contour integral since both the functions $\partial F/\partial z^* = 1/(z - z_0)$ and $F(z) = (z - z_0)^*/(z - z_0)$ (equ. 45) have singularity in $z = z_0$. This problem can be solved for all points inside the coil introducing an equivalent (in the sense of having the same values) analytic function.

For each point inside the coil (excluding the boundary) it is possible to remove a circle (δ), with infinitesimal area, centered in z_0 and completely contained in the coil (see fig. 8). Calling $B_2(z)$ the magnetic field generated by a coil whose section is $\sigma - \delta$, and $B(z)$ the field generated by the whole coil (with section σ), it is $B_2^*(z_0) = B^*(z_0)$ because the magnetic field generated by a circularly-shaped uniform current distribution is zero in its center. When calculating $B_2(z_0)$ it's possible to use the Green's theorem because z_0 is no longer inside the new coil (that is $\sigma - \delta$). The integrand ($F(z)$) can be every function of this kind: $F(z) = z^*/(z - z_0) + g$, where g is a generic function with $\partial g/\partial z^* = 0$. The field is then

$$B_2^*(z_0) = \frac{\mu_0 J}{4\pi} \int_{\gamma_1+\gamma_2} \left(\frac{z^*}{z - z_0} + g\right) dz \tag{48}$$

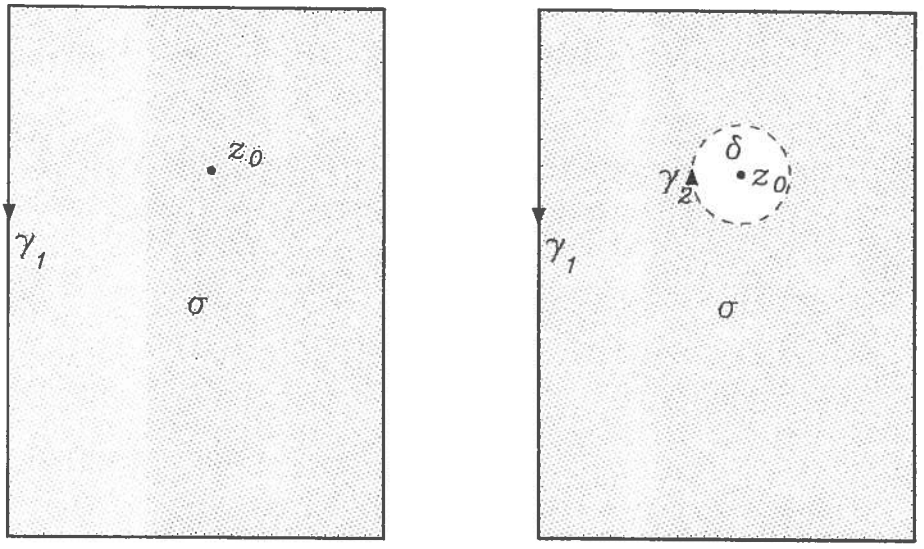

FIG. 8: Integration contour used to calculate the field inside a coil. See text for details.

where the integral must be covered in anticlockwise direction along γ_1 and in clockwise direction along γ_2. It is possible to simplify the calculation of the integral using the particular form of the function $g = -z_0^*/(z - z_0)$. In this case

$$\int_{\gamma_2} \frac{z^* - z_0^*}{z - z_0}\, dz = ir \int_{2\pi}^{0} e^{-i\theta}\, d\theta = 0 \tag{49}$$

The magnetic field in each point inside the coil, but not on its boundary, is therefore given by a contour integral along the boundary (γ_1) of the coil (σ)

$$B^*(z_0) = B_3^*(z_0) \stackrel{\text{def}}{=} \frac{\mu_0 J}{4\pi} \int_{\gamma_1} \frac{z^* - z_0^*}{z - z_0}\, dz. \tag{50}$$

The function $B_3^*(z_0)$ has another very important characteristic: it is analytic for all points z_0 outside or inside the coil, but not on its boundary. This result can be demonstrated[7] in a formal way since $B_3^*(z_0)$ is a function of the kind

$$\int_{\gamma} \frac{f(z)}{g(z) - z_0}\, dz; \tag{51}$$

moreover the function $B_3^*(z_0)$ is continuous across the boundary and therefore the magnetic field can be calculated also on the boundary.

The peak field on a coil is in general due to the self-field of the coil and to the field of all the other coils, including the image coils generated by the iron yoke. The total field is then the sum of functions which are analytic inside the given coil; follows that the peak field (maximum value of the modulus) must be on the boundary of the coil.

Also the force acting on a coil can be calculated with a contour integral[3] . Setting $f^* = f_x - i f_y$ (f_x and f_y are the force components per meter length) it is:

$$f^* = -\frac{i\mu_0}{2} \oint_{\gamma} H^{*2}\, dz, \tag{52}$$

where γ can be every contour containing the coil and contained in the aperture.

9 EXAMPLES

9.1 Line integrals

Coil boundaries can usually be described with straight lines and/or circular arcs. Here we give some examples of integrals along these paths, useful for the calculation of the multipole coefficients and magnetic field for the most general coil shape.

Segment parallel to axes

For a segment parallel to the X-axis it is $dz = dx + idy = dx$. We start considering the integral in equ. 42 for multipole coefficients and magnetic field calculation. Setting $z_1 = x_1 + ih$ and $z_2 = x_2 + ih$ the segment extremes and defining:

$$I_n = \int_{z_1}^{z_2} \frac{z^*}{z^n}\, dz = \int_{x_1}^{x_2} \frac{x}{(x+iy)^n}\, dx - ih \int_{x_1}^{x_2} \frac{1}{(x+iy)^n}\, dx \tag{53}$$

then it is:

$$\begin{aligned} I_1 &= [x - ih\, ln(x+ih)]_{x_1}^{x_2} - ih\, [ln(x+ih)]_{x_1}^{x_2} \\ &= (x_2 - x_1) - 2ih\, ln\left(\frac{z_2}{z_1}\right) \end{aligned} \tag{54}$$

$$\begin{aligned} I_2 &= \left[\frac{ih}{x+ih} + ln(x+ih)\right]_{x_1}^{x_2} - ih\left[-\frac{1}{x+ih}\right]_{x_1}^{x_2} \\ &= 2ih\left(\frac{1}{z_2} - \frac{1}{z_1}\right) + ln\left(\frac{z_2}{z_1}\right) \end{aligned} \tag{55}$$

$$\begin{aligned} I_{n>2} &= \left[\frac{1}{2-n}\frac{1}{(x+ih)^{n-2}} - \frac{ih}{1-n}\frac{1}{(x+ih)^{n-1}}\right]_{x_1}^{x_2} - ih\left[\frac{1}{1-n}\frac{1}{(x+ih)^{n-1}}\right]_{x_1}^{x_2} \\ &= \frac{1}{2-n}\left(\frac{1}{z_2^{n-2}} - \frac{1}{z_1^{n-2}}\right) - \frac{2ih}{1-n}\left(\frac{1}{z_2^{n-1}} - \frac{1}{z_1^{n-1}}\right) \end{aligned} \tag{56}$$

To obtain the iron contribution to the field, the integral in equ. 47 should be used. On this segment it becomes:

$$\begin{aligned} &\int_{x_1}^{x_2} \frac{x^2 + h^2}{R^2 - z_0(x - ih)}\, dx \\ &= -(x_2 - x_1)\left(\frac{z_2 + z_1}{2z_0} + \frac{R^2}{z_0^2}\right) - \left(\frac{R^4}{z_0^3} + \frac{2ihR^2}{z_0^2}\right) ln\left(\frac{R^2 - z_0 z_2^*}{R^2 - z_0 z_1^*}\right) \end{aligned} \tag{57}$$

The integrals for the computation of the iron contribution to multipoles, not reported for this example, can be obtained from the following general case.

Any segment

For this case we solve the path integrals for multipole coefficients and magnetic field calculation both with and without iron. Setting the segment extremes $z_1 = x_1 + iy_1$

and $z_2 = x_2 + iy_2$, the integral in equ. 42 with n=1 (for dipole coefficient) along a generic segment is:

$$\int_{z_1}^{z_2} \frac{z^*}{z}\, dz \tag{58}$$

The segment can be parameterized as :

$$z(t) = z_1 + (z_2 - z_1)t \quad (0 \le t \le 1) \tag{59}$$

and the integral becomes:

$$\int_0^1 \frac{z_1^* + (z_2^* - z_1^*)t}{z_1 + (z_2 - z_1)t}(z_2 - z_1)\, dt$$

$$= z_1^* \left[ln(z_1 + (z_2 - z_1)t)\right]_0^1 + (z_2 - z_1)(z_2 - z_1)^* \left[\frac{t}{z_2 - z_1} - \frac{z_1}{(z_2 - z_1)^2} ln(z_1 + (z_2 - z_1)t)\right]_0^1$$

$$= ln\left(\frac{z_2}{z_1}\right)\left(z_1^* - z_1\frac{(z_2 - z_1)^*}{z_2 - z_1}\right) + (z_2 - z_1)^* \quad (c_1) \tag{60}$$

Using the same parameterization in equ. 43, for the other multipole coefficients calculation, and in equ. 44 for the iron contribution to multipoles, we have:

$$\int_{z_1}^{z_2} \frac{1}{z}\, dz^* = ln\left(\frac{z_2}{z_1}\right)\frac{(z_2 - z_1)^*}{z_2 - z_1} \quad (c_2) \tag{61}$$

$$\int_{z_1}^{z_2} \frac{1}{z^{n-1}}\, dz^* = \left(\frac{z_2^{2-n} - z_1^{2-n}}{2 - n}\right)\frac{(z_2 - z_1)^*}{z_2 - z_1} \quad (c_{n>2}) \tag{62}$$

$$\int_{z_1}^{z_2} (z^*)^{n+1}\, dz = \left(\frac{(z_2^*)^{n+2} - (z_1^*)^{n+2}}{n + 2}\right)\frac{z_2 - z_1}{(z_2 - z_1)^*} \quad (c_{n,iron}) \tag{63}$$

The path integral to calculate the magnetic field of the coil is:

$$\int_{z_1}^{z_2} \frac{z^* - z_0^*}{z - z_0}\, dz$$

$$= ln\left(\frac{z_2 - z_0}{z_1 - z_0}\right)\left((z_1^* - z_0^*) - (z_1 - z_0)\frac{(z_2 - z_1)^*}{z_2 - z_1}\right) + (z_2 - z_1)^* \tag{64}$$

We point out that when the field point z_0 is on the segment the integral gives the result $(z_2 - z_1)^*$.

The path integral useful to calculate the iron contribution to the magnetic field in z_0 (equ. 47) is:

$$\int_{z_1}^{z_2} \frac{zz^*}{R^2 - z_0 z^*}\, dz^*$$

$$= \frac{1}{2z_0}(z_1^* - z_2^*)(z_2 + z_1) - \frac{1}{z_0^2}R^2(z_2 - z_1) + ln\left(\frac{R^2 - z_0 z_2^*}{R^2 - z_0 z_1^*}\right)\cdot\left(\frac{R^4(z_2 - z_1) + R^2 z_0(z_2^* z_1 - z_1^* z_2)}{z_0^3(z_1 - z_2)^*}\right) \tag{65}$$

Circular arc with center in the origin

Here we report the path integrals for a circular arc of radius r with center in the origin. Setting the path ends $z_1 = re^{i\theta_1}$ and $z_2 = re^{i\theta_2}$ the expression useful to calculate multipole coefficients are:

$$\int_{z_1}^{z_2} \frac{z^*}{z}\, dz = ir \int_{\theta_1}^{\theta_2} e^{-i\theta}\, d\theta = -r\left(e^{-i\theta_2} - e^{-i\theta_1}\right) = -(z_2^* - z_1^*) \quad (c_1) \tag{66}$$

$$\int_{z_1}^{z_2} \frac{1}{z^{n-1}}\, dz^* = \frac{1}{nr^{2(n-1)}}((z_2^*)^n - (z_1^*)^n) \quad (c_{n\geq 2}) \tag{67}$$

$$\int_{z_1}^{z_2} (z^*)^{n+1}\, dz = -\frac{r^2}{n}((z_2^*)^n - (z_1^*)^n) \quad (c_{n,iron}) \tag{68}$$

To calculate the magnetic field due to the coil:

$$\int_{z_1}^{z_2} \frac{z^* - z_0^*}{z - z_0}\, dz = \left(\frac{r^2}{z_0} - z_0^*\right) ln\left(\frac{z_2 - z_0}{z_1 - z_0}\right) - \frac{r^2}{z_0} ln\left(\frac{z_2}{z_1}\right) \tag{69}$$

When the field point z_0 is on the segment the integral gives the result $-z_0^*\, ln(z_2/z_1)$. The contribution to the field due to the iron shield is:

$$\int_{z_1}^{z_2} \frac{zz^*}{R^2 - z_0 z^*}\, dz^* = \frac{r^2}{z_0} ln\left(\frac{R^2 - z_0 z_1^*}{R^2 - z_0 z_2^*}\right) \tag{70}$$

9.2 Coil examples

In this section we report magnetic field and multipole coefficients calculation for some kinds of coils. The closed formulas are obtained assembling the path integrals previously reported.

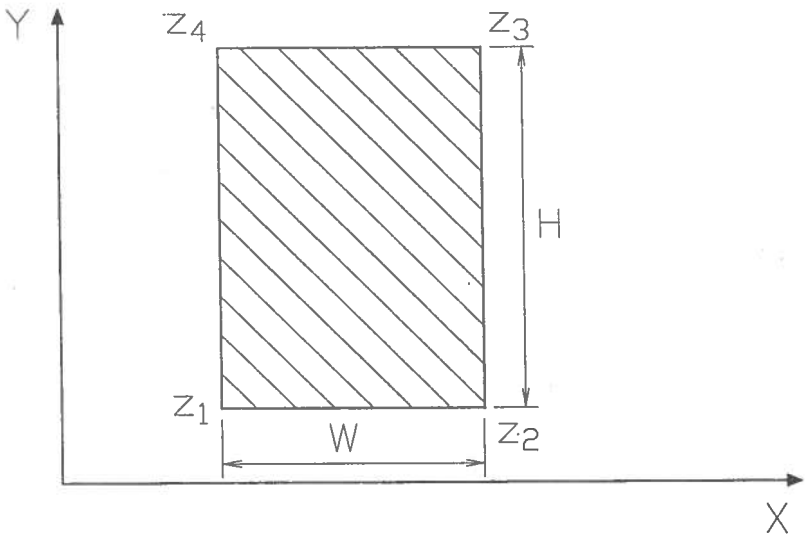

FIG. 9: Rectangular coil with sides parallel to axes.

Rectangular coils with sides parallel to axes

The multipole coefficients for a coil of this kind with midplane symmetry have been reported in sections 6. Here we report the results for any rectangular coil with sides parallel to axes. We start using equ. 42 with n=1 to obtain the dipole coefficient (c_1). The integrals along the horizontal paths are given by equ. 54, while the others are given by a similar formula for segments parallel to the Y-axis. Referring to fig. 9 for symbols, it is:

$$c_1 = \frac{\mu_0 J}{4\pi}\int_\gamma \frac{z^*}{z}\,dz$$

$$= \frac{\mu_0 J}{4\pi}\left[(x_2-x_1) - 2iy_1\, ln\left(\frac{z_2}{z_1}\right) - i(y_3-y_2) + 2x_2\, ln\left(\frac{z_3}{z_2}\right) + \right.$$

$$\left.(x_4-x_3) - 2iy_3\, ln\left(\frac{z_4}{z_3}\right) - i(y_1-y_4) + 2x_4\, ln\left(\frac{z_1}{z_4}\right)\right]$$

$$= \frac{\mu_0 J}{2\pi}\sum_{k=1}^{4}[(-1)^{k+1} z_k ln(z_k)] \tag{71}$$

The method to obtain the other multipole coefficients from equ. 42 is just the same using equations 55 and 56.

$$c_2 = \frac{\mu_0 J}{2\pi} ln\left(\frac{z_2 z_4}{z_1 z_3}\right) \tag{72}$$

$$c_{n>2} = \frac{\mu_0 J}{2\pi}\frac{1}{(n-1)(n-2)}\sum_{k=1}^{4}\left[(-1)^{k+1}\frac{1}{z_k^{n-2}}\right] \tag{73}$$

Also the contribution to multipoles of a circular iron screen can be calculated in the same way using equ. 63 in equ. 44[1]. In case of an infinite iron permeability it is:

$$c_{n,iron} = \frac{\mu_0 J}{4\pi}\frac{1}{(n+1)R^{2n}}\int_\gamma (z^*)^{n+1}\,dz$$

$$= \frac{\mu_0 J}{4\pi}\left\{\frac{[(z_2^*)^{n+2}-(z_1^*)^{n+2}] - [(z_3^*)^{n+2}-(z_2^*)^{n+2}] + [(z_4^*)^{n+2}-(z_3^*)^{n+2}] - [(z_1^*)^{n+2}-(z_4^*)^{n+2}]}{(n+1)(n+2)R^{2n}}\right\}$$

$$= \frac{\mu_0 J}{2\pi}\left\{\frac{-(z_1^*)^{n+2} + (z_2^*)^{n+2} - (z_3^*)^{n+2} + (z_4^*)^{n+2}}{(n+1)(n+2)R^{2n}}\right\} \tag{74}$$

[1]Equ. 35 can be derived from equ. 74 considering that for a coil symmetric to X-axis, using polar coordinates

$$c_{n,iron} = \left(\frac{\mu_r-1}{\mu_r+1}\right)\frac{\mu_0 J}{2\pi}\left\{\frac{-(r_1 e^{i\alpha_1})^{n+2} + (r_2 e^{i\alpha_2})^{n+2} - (r_2 e^{-i\alpha_2})^{n+2} + (r_1 e^{-i\alpha_1})^{n+2}}{(n+1)(n+2)R^{2n}}\right\}$$

$$= \left(\frac{\mu_r-1}{\mu_r+1}\right)\frac{\mu_0 J}{2\pi}\left\{\frac{r_2^{n+2}2isin[(n+2)\alpha_2] - r_1^{n+2}2isin[(n+2)\alpha_1]}{(n+1)(n+2)R^{2n}}\right\}$$

Magnetic field can be easily calculated. By means of the variable change $\zeta = z - z_0$ equ. 45 becomes equal to equ. 42 with n=1, whose result for this coil is shown in equ. 71. Therefore the magnetic field is:

$$B^*(z_0) = \frac{\mu_0 J}{2\pi} \sum_{k=1}^{4} [(-1)^{k+1}(z_k - z_0) ln(z_k - z_0)] \tag{75}$$

The iron contribution to the field can be obtained applying the result of equ. 57 to equ. 47. Before adding all pieces it should be noted that $z_3 + z_4 - z_2 - z_1 = 2i(y_3 - y_2) = 2iH$ and that getting together all pieces like $ln(R^2 - z_0 z_k^*)$ it is:

$$ln(R^2 - z_0 z_k^*)(R^4 - 2z_0 R^2 x_k + R^4 + 2iz_0 R^2 y_k) = 2R^2(R^2 - z_0 z_k^*) ln(R^2 - z_0 z_k^*) \tag{76}$$

Therefore the result is

$$\begin{aligned} B^*_{iron}(z_0) &= -\left(\frac{\mu_r - 1}{\mu_r + 1}\right) \frac{\mu_0 J}{2\pi} \left\{ \frac{i}{z_0} WH + \frac{R^2}{z_0^3} \sum_{k=1}^{4} [(-1)^{k+1}(R^2 - z_0 z_k^*) ln(R^2 - z_0 z_k^*)] \right\} \\ B^*_{iron}(0) &= \left(\frac{\mu_r - 1}{\mu_r + 1}\right) \frac{\mu_0 J}{4\pi} \frac{iWH}{R^2} (z_1^* + z_3^*) \end{aligned} \tag{77}$$

Circular shell coils

The multipole coefficients for this kind of coils can be easily calculated, and have already been reported in case of a coil with midplane symmetry. Here we report the formulas useful to calculate multipole coefficient and magnetic field, both with and without iron shield, for a coil whose vertices are: $z_1 = r_1 e^{i\alpha}$, $z_2 = r_2 e^{i\alpha}$, $z_3 = r_2 e^{i\beta}$, $z_4 = r_1 e^{i\beta}$ (see fig. 10).

$$c_1 = \frac{\mu_0 J}{2\pi} (r_2 - r_1) \left(e^{-i\alpha} - e^{-i\beta}\right) \tag{78}$$

$$c_2 = \frac{\mu_0 J}{4\pi} ln\left(\frac{r_2}{r_1}\right) \left(e^{-2i\alpha} - e^{-2i\beta}\right) \tag{79}$$

$$c_{n>2} = \frac{\mu_0 J}{2\pi} \frac{1}{n(n-2)} \left(\frac{1}{r_2^{n-2}} - \frac{1}{r_1^{n-2}}\right) \left(e^{-ni\beta} - e^{-ni\alpha}\right) \tag{80}$$

$$c_{n,iron} = \left(\frac{\mu_r - 1}{\mu_r + 1}\right) \frac{\mu_0 J}{2\pi} \frac{1}{n(n+2)R^{2n}} \left(r_2^{n+2} - r_1^{n+2}\right) \left(e^{-ni\alpha} - e^{-ni\beta}\right) \tag{81}$$

$$\begin{aligned} B^*(z_0) = \frac{\mu_0 J}{4\pi} \Bigg\{ & (e^{-i\alpha} - e^{-i\beta})(r_2 - r_1) - \frac{i(\beta - \alpha)}{z_0} (r_2^2 - r_1^2) \\ & - \frac{1}{z_0} \sum_{k=1}^{4} \left[(-1)^k ln(z_k - z_0) z_k z_k^* \left(1 - \frac{z_0^2}{z_k^2}\right) \right] \Bigg\} \end{aligned} \tag{82}$$

$$B^*(0) = c_1 \tag{83}$$

$$\begin{aligned} B^*_{iron}(z_0) = \left(\frac{\mu_r - 1}{\mu_r + 1}\right) \frac{\mu_0 J}{4\pi} \Bigg\{ & \frac{R^2}{z_0^2} (e^{-i\alpha} - e^{-i\beta})(r_2 - r_1) \\ & + \frac{1}{z_0} \sum_{k=1}^{4} \left[(-1)^{k+1} ln(R^2 - z_k^* z_0) z_k z_k^* \left(1 - \frac{R^4}{z_0^2 (z_k^*)^2}\right) \right] \Bigg\} \end{aligned} \tag{84}$$

$$B^*_{iron}(0) = c_{1,iron} \tag{85}$$

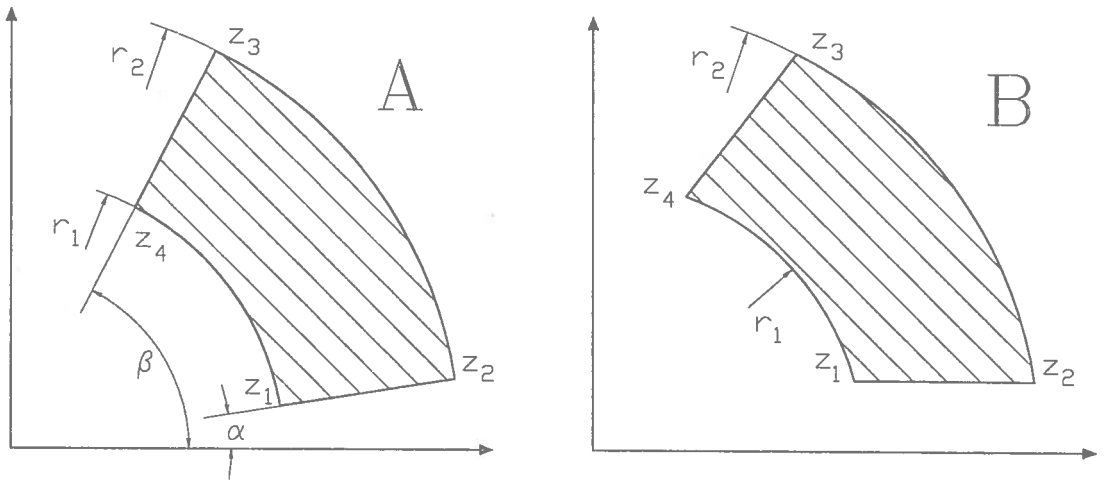

FIG. 10: A: Circular shell coil; B: Slanted shell coil.

Slanted shell coils

These coils have two sides made by circular arcs, with center in the origin, whose ends are connected by straight lines (see fig. 10). In circular shell coils the straight sides point to the origin, while in slanted shell coils this condition is removed.

A shell coil made of a keystoned cable and/or wedges can be well approximated with a slanted shell coil with uniform current density.

For this kind of coils it is useless to search for compact formulas to calculate multipole coefficients or magnetic field: each result should be obtained adding all path integrals (presented in sect. 9.1) along coil boundary.

9.3 Calculation warnings

Magnetic field computation inside a coil and in some regions outside it may give problems. This is due to the differences between logarithms that appear in some formulas, since the function lnz has a discontinuity line. In fact it is $lnz = ln(\rho e^{i\theta}) = i\theta + ln\rho$ where θ is the argument of the complex number z, and the function argument has a discontinuity line. Usually this is set on the real axis from 0 to $-\infty$ and the argument range is $-\pi < \theta \leq \pi$.

Therefore the result of a path integral containing a difference between logarithms is correctly computed only if the path doesn't cross the discontinuity line. Otherwise the result contains an "extra term" $(2\pi i)$ due to the crossing of the discontinuity line. For instance if the path is like l_1 in fig. 11 it is

$$(ln\ z_B - ln\ z_A) = ln\left(\frac{\rho_B}{\rho_A}\right) + i(\theta_B - \theta_A) \tag{86}$$

with the arguments $-\pi < \theta_A < \theta_B \leq \pi$. Instead when the path crosses the discontinuity line, as l_2 in the same figure, the position of the discontinuity line has to be changed. For instance it can be set on the positive part of the real axis increasing of 2π all arguments $\theta \leq 0$.

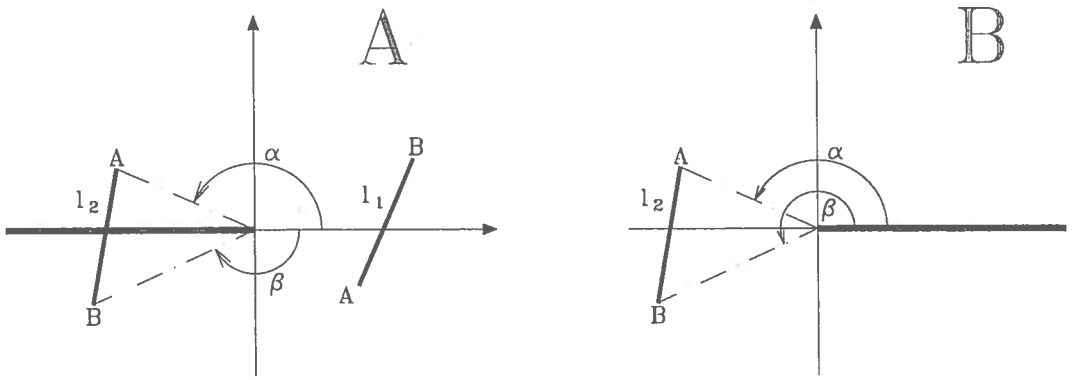

FIG. 11: Two different discontinuity line positions for the function ln z to calculate the path integral along l_1 (fig A) and along l_2 (fig B).

This change can be implemented in a computer program with a simple routine executed before calculating the path integral. In this way all problems that may arise from the calculus of a specific path integral are solved.

Attention must be paid when using compact formulas to calculate the field. The variable change $\zeta = z - z_0$ translates the axes origin in z_0. Therefore when the field is calculated inside a coil every position of the discontinuity line crosses at least one coil side.

In this case there are two possibilities:

- to change the argument range according to the position of each path before the integration along it, adding at the end all the results;
- to look for a set of compact formulas in order to have at least one formula usable in each point. In this way the plane is divided into regions depending on which coil side is cut by the discontinuity line when z_0 belongs to a region.

The first technique can be used for every kind of coil, while the second may need many compact formulas depending on the position of coil sides.

As an example of the second technique here we report two formulas to compute the field of a rectangular coil with sides parallel to the axes.

Inside the coil the field is given by the following formula using the normal range of the arguments $(-\pi < \theta \leq \pi)$

$$B^*(z_0) = \frac{\mu_0 J}{2\pi}\left\{\sum_{k=1}^{4}[(-1)^{k+1}(z_k - z_0)ln(z_k - z_0)] + 2\pi i(x_1 - x_0)\right\} \qquad (87)$$

Next expression can be used for all points with $x \geq x_2$ (see fig. 9) changing the argument range: $0 < \theta \leq 2\pi$; otherwise it can be used in all the other points outside the coil, with the normal argument range: $-\pi < \theta \leq \pi$;

$$B^*(z_0) = \frac{\mu_0 J}{2\pi}\sum_{k=1}^{4}[(-1)^{k+1}(z_k - z_0)ln(z_k - z_0)] \qquad (88)$$

When magnetic field is to be calculated in a point on a coil side parallel to Y-axis both the formulas of the adjacent regions can be used. In fact these expressions are

continues functions when z_0 crosses these coil sides. On the contrary only one formula is correct on the horizontal boundaries. If the θ range is $-\pi < \theta \leq \pi$ then equation 87 must be used on the upper side while equation 88 should be used on the lower.

Logarithms appear also in some formulas for the calculus of multipolar coefficients. No problems arise if the coil is in the first quadrant. Attention must be paid only if the coil cuts the negative part of the real axis.

10 A TEST CASE: RESULTS AND COMPARISONS

The analytical formulas, based on the complex contour integration technique, presented in this report have been incorporated in the code QCSL for the computation of the multipole coefficients and of the peak field on coils for superconducting magnet with midplane and azimuthal symmetries. The code QCSL is extremely fast and it has been used in the initial design stage of a superconducting quadrupole [1] .

The effects of the two main approximations of the code (constant current density in the coil and constant permeability of the cylindrical iron yoke) have been checked with two different codes:

- ROXIE[8] , an analytical program with a detailed simulation of the cables (and constant iron permeability)
- POISSON[9] , a magnetostatic code which takes into account the real iron permeability (with uniform current density in the coils)

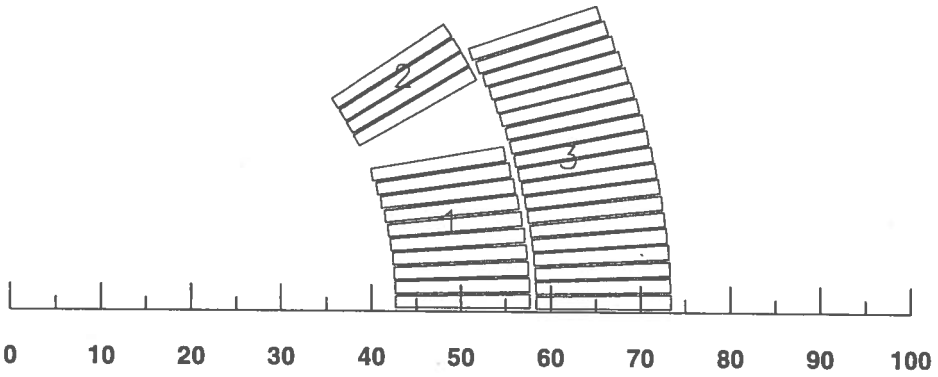

FIG. 12: Coil layout of the test case produced by $\text{ROXIE}_{3.6}$.

The test case is a two shells superconducting quadrupole with a 85 mm aperture. Data on coil and iron structure and on the NbSn cable are given respectively in table 1 and table 2. An octant of the coil structure is shown in fig. 12 where is also visible the cables layout.

In ROXIE the position of every cable is calculated piling up all the cables, starting from the midplane (or any given plane), taking into account the insulation and keeping them in contact with the winding mandrel. The magnetic field is generated by current filaments that are placed regularly in each cable [8] . The current flowing in each filament can be constant (giving a grading of the current density inside a keystoned

TABLE 1: *Coils characteristics*

	inner radius (mm)	outer radius (mm)
coil 1	42.5	57.5
coil 2	42.5	57.5
coil 3	58.2	73.2
ROXIE iron	93.4	∞
POISSON iron	93.4	214
QCSL iron	93.4	∞

TABLE 2: *Cable characteristics.*

width (bare) (mm)	15
inner thickness (bare) (mm)	1.60
outer thickness (bare) (mm)	1.34
azimuthal insulation (mm)	0.125
radial insulation (mm)	0.2
number of strands	36
strand diameter (mm)	0.825
Cu/NoCu ratio	1.1/1
J_c at 14 T 1.9 K (A/mm^2)	1266
$\Delta J_c/\Delta B$ (A/mm^2 T)	272
current (A)	15570

cable) or can be set proportional to the cable thickness (to simulate a uniform current density distribution).

Multipole coefficients are obtained through a Fourier analysis of the magnetic field at a specified radius in the aperture. The peak field in the coils is searched along the cables boundaries and in the points between every couple of adjacent current filaments.

The peak field can be calculated with or without the self-field of the nearest current filament in order to have a better comparison with critical current measurements, that usually do not take into account the self-field of the sample. In this comparison the peak field includes the self field.

The code QCSL calculates directly the multipole coefficients and peak field of rectangular or shell coils. The dimension of the coil is given by the stack of cables with their azimuthal insulation (but without the radial), then forming a slanted shell coil. The value used for the current density (J) is the total current of the cables (I) divided the coil surface.

The results of the comparison, reported in table 3, show that:

- constant current density in the cables gives -0.6 % less gradient and 3.0 10^{-6} on B_6 respect to the grading of the current in the cable as deduced by the two ROXIE cases. The peak field value is instead equal,
- QCSL gives gradient close to ROXIE, -0.35 %, but for B_6 there is a difference

TABLE 3: *ROXIE - QCSL comparison*

	QCSL		ROXIE	
normal	227.4	b_2 (T/m)	228.2	normal
	7.8	B_6 (10^{-6} T)	0.6	
	0.017	B_{10} (10^{-6} T)	0.03	
	11.10	B_{peak} (T)	11.171	
	93.00	J/J_c (%)	93.36	
		b_2 (T/m)	226.8	without
		B_6 (10^{-6} T)	3.5	current grading
		B_{10} (10^{-6} T)	0.04	due to keystone
		B_{peak} (T)	11.167	
		J/J_c (%)	93.34	

of 7 10^{-6} (and smaller difference in B_{10}). Half of the difference is due to the constant current density approximation and half is given by azimuthal insulation (included in the coil by QCSL) that is quite important on coil sides because they are carefully positioned to minimize high order multipoles,

- the peak field value found by QCSL is lower by 0.6 % and this gives a 0.36 % more margin on the load line.

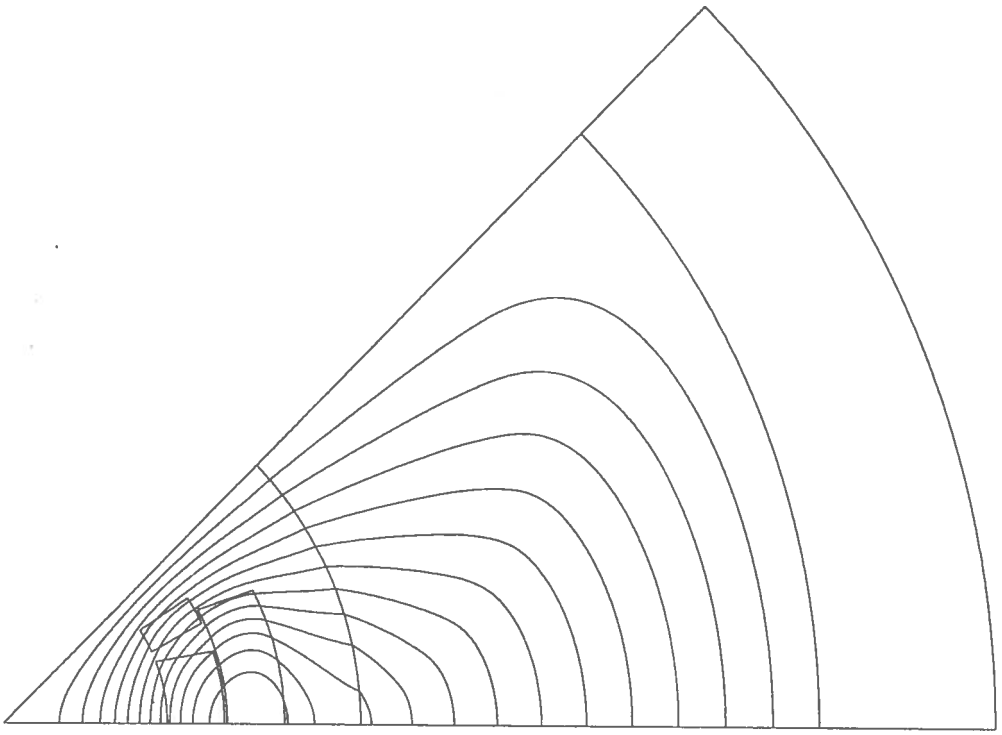

FIG. 13: POISSON flux plot for the test case.

The effects of the constant iron permeability approximation can be seen comparing

TABLE 4: *POISSON - QCSL comparison*

	QCSL		POISSON	
$\mu = \infty$	235.45	b_2 (T/m)	235.47	$\mu = \infty$
	44.6	B_6 (10^{-6} T)	48.8	
	0.08	B_{10} (10^{-6} T)	0.17	
	11.45	B_{peak} (T)	11.20	
$\mu = 6$	226.27	b_2 (T/m)	225.77	$\mu = 6$
	44.5	B_6 (10^{-6} T)	48.6	
	0.08	B_{10} (10^{-6} T)	0.17	
	11.00	B_{peak} (T)	10.72	
$\mu = 5$	224.75	b_2 (T/m)	224.72	$\mu =$ table
	44.4	B_6 (10^{-6} T)	53.2	
	0.08	B_{10} (10^{-6} T)	0.17	
	10.92	B_{peak} (T)	10.66	

QCSL results with POISSON. The test case (see fig. 13) is a two shells coil with a wedge, like the coil used in the previous case, and with a uniform current density.

POISSON runs have been done also at $\mu = \infty$ and $\mu = 6$ in order to show respectively the 'systematic errors' of POISSON and the effects of the outer radius of the yoke (ignored in QCSL) We recall that POISSON has no possibility to search automatically for the peak field value in the coils, and moreover the field interpolation routine has some troubles, at least in the version we used, near the coil boundary. The results of the comparison, reported in table 4, show that:

- the peak field found with POISSON is lower than the true (found analytically in the case $\mu = \infty$) with an error $\Delta B/B = -2.2$ %,
- the gradient is the same ($\Delta G/G = 10^{-4}$) in case of $\mu = \infty$, while there is a small difference ($\Delta G/G = 2.2\ 10^{-3}$) in case of $\mu = 6$ due to the infinite external radius of the iron assumed by QCSL,
- the B_6 found with POISSON is greater than the true (found analytically) of about $\Delta B_6 = 4\ 10^{-6}$ (this is more an absolute error than a relative one because it almost doesn't change if the magnitude of B_6 is changed). The systematic error on B_{10} is of the order of 10^{-7},
- having found the 'systematic errors' of POISSON a constant value for the iron permeability, $\mu = 5$, was fitted to obtain in QCSL the same gradient of POISSON with the real iron permeability. The difference in B_6 is $9\ 10^{-6}$ is part due to systematic errors ($4\ 10^{-6}$) and part ($5\ 10^{-6}$) to the differential saturation of the iron. The peak field value show almost the systematic difference ($2\ 10^{-2}$) and no influence is seen on B_{10} from the iron saturation

Considering the results of these comparisons it can be said that an analytical program using formulas like those here reported, approximating the coils with uniform current density distributions and the iron with an 'average' constant permeability, is

a fast and useful tool to calculate multipole coefficients and peak field on coils of a superconducting magnet, at least for quadrupoles.

The precision in high order multipoles (of the order of few 10^{-6}) may not be sufficient for the final design (for instance all undesired multipoles should be equal to, or lower than, few 10^{-6} in the *low* β quadrupole of LHC). The effects due to the iron saturation and to the true iron shape can be studied only with a numerical code, but it's quite difficult to put into it a precise coils geometry (i.e. the insulated cables piled and fitted against the mandrel) and the absolute precision of a numerical code is questionable (as we have shown in the case of B_6 and peak field by POISSON).

A solution is to use an analytical program considering all the effects due to cables position (like ROXIE does, but it can be done also by a program using the contour integral technique), using an 'average' constant iron permeability, and finally adding to its results the relative variations due to iron saturation and shape.

11 CONCLUSION

Analytical formulas have been presented for the calculation of the fundamental parameters of a superconducting accelerator magnet, namely the multipole coefficients in the aperture and the peak field (that sets the critical current) in the coils.

Explicit formulas for the multipole coefficients have been given for the simplest coil configuration (rectangular or shell) and a general technique has been indicated for the most general coil shape.

It has been also shown that the peak field on the coils is reached on the boundary therefore simplifying considerably the search process to evaluate the peak value.

A test case shows that the two basic assumptions (constant current density in the coils and constant iron permeability) give quite small errors on the computed multipole coefficients and on the peak field value on the coils.

REFERENCES

(1) G. Ambrosio, G. Bellomo, and L. Rossi *"A 300 T/m Nb_3Sn quadrupole for the low β insertions of the LHC"*, to be published in Proc. of EPAC96, 10-14 June 1996, Sitges (Barcelona);
G. Ambrosio, G. Bellomo, and L. Rossi *"Study of a high gradient, large aperture Nb_3Sn quadrupole for the low β insertions of the LHC"*, Proc. of EPAC94, London (1994), p. 2268;
G. Ambrosio, F. Ametrano, G. Bellomo, F. Broggi, L. Rossi, G. Volpini *"Preliminary proposal of a Nb_3Sn quadrupole model for the low β insertions of the LHC"*, INFN/TC-95/25 (1995).

(2) R. Beth *"Complex representation and computation of two-dimensional magnetic fields"*, Journal of Applied Physics 37(7) (1966) p. 2568;
R. Beth *"An integral formula for two-dimensional fields"*, Journal of Applied Physics 38(12) (1967) p. 4689;
R. Beth *"Evaluation of current-produced two-dimensional magnetic fields"*, Journal of Applied Physics 40(12) (1969) p. 4782.

(3) K. Halbach *"Fields and first order perturbation effects in two-dimensional conductor dominated magnets"*, NIM 78 (1970) p. 196.

(4) H. Brechna *"Superconducting Magnet Systems"*, Springer-Verlag Berlin (1973), chapter II.

(5) K.H. Meb, P. Schmuser *"Superconducting accelerator magnets"*, Report CERN 89-04 (1989), p. 87.

(6) R. Perin *"Calculation of magnetic field in a cylindrical geometry produced by sector or layer windings"*, Internal note CERN ISR-MA/RP/cb/ (1973)

(7) M.R. Spiegel *"Complex variables"*, Schaum series, McGraw-Hill.

(8) S. Russenschuck *"ROXIE "*, Internal note CERN AT/93-27 (1993)

(9) *"POISSON"*, Los Alamos Report LA-UR-126 (1987)